

## Supplementary Information

# Thermo-Sensitive Discotic Colloidal Liquid Crystals

Xuezhen Wang<sup>a</sup>, Di Zhao<sup>b</sup>, Agustin Diaz<sup>c</sup>, Ilse Nava Medina<sup>d</sup>, Huiliang Wang<sup>b</sup>, Zhengdong Cheng<sup>ade</sup>

<sup>a</sup>Artie McFerrin Department of Chemical Engineering, Texas A&M University, College Station, TX, 77843-3122, USA. E-mail: zcheng@tamu.edu

<sup>b</sup>College of Chemistry, Beijing Normal University, Beijing, 100875, China

<sup>c</sup>Department of Chemistry, Texas A&M University, College Station, TX 77843-3125, USA.

<sup>d</sup>Materials Science and Engineering, Texas A&M University, College Station, TX, 77843-3003, USA

<sup>e</sup>Mary Kay O'Connor Process Safety Center, Artie McFerrin Department of Chemical Engineering, Texas A&M University, College Station, TX, 77843-3122, USA

<sup>f</sup>Soft Matter Center, Guangdong Provincial Key Laboratory on Functional Soft Condensed Matter, School of materials and energy, Guangdong University of Technology, Guangzhou, 510006, China

## 1. Pristine $\alpha$ -ZrP

Pristine  $\alpha$ -ZrP is shown in Fig. S1. After exfoliation by TBAOH, the particle was exfoliated into many hexagonal monolayers.<sup>1</sup> Platelet size used for the later calculations was measured by dynamic light scattering (DLS).

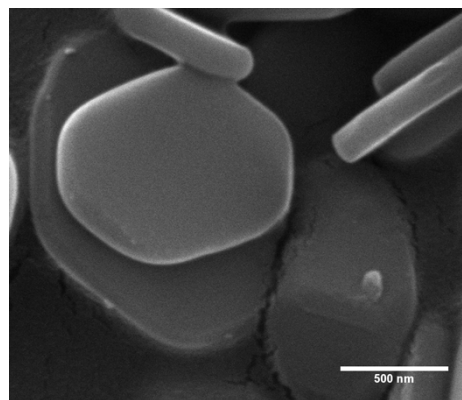


Fig. S1 SEM image of the pristine  $\alpha$ -ZrP.

## 2. Grafting PNIPAM to ZrP platelets by pre-irradiated polymerization

To determine the amount of peroxides produced on the ZrP platelet surface, the classical iodometric method was performed.<sup>2</sup> 2 mL of irradiated ZrP suspension was injected into a 50-mL round-bottom three-neck flask, followed by injection of 10 mL of isopropyl alcohol, and further bubbled with nitrogen for 15 minutes to remove air before 0.3 g of NaI was added. The suspension was heated and refluxed for 30 minutes. After the reaction, the yielded suspension

was diluted to a total volume of 100 mL. The molar concentration of  $I^{3-}$  formed was measured with a UV-Vis spectrometer (Shimadzu UV-1800). As a control experiment, a ZrP platelet suspension without gamma irradiation was also reacted with NaI, diluted, and measured with UV-Vis as well.

Fig. S2 shows the UV-Vis spectra of the amount of iodine produced using the gamma-irradiated ZrP platelets and the control sample with non-irradiated ZrP platelets. After reacting with NaI, the peaks at 293 nm and 361 nm indicate the existence of  $I_2$ , which is produced by oxidation of  $I^-$ . The absorption peaks show that the amount of  $I_2$  produced by gamma-irradiated ZrP platelets (solid line) is much greater than the amount of  $I_2$  produced by the control (dashed line). The small absorption peaks of the dashed line might be due to the oxygen from the air, which can oxidize some  $I^-$  to  $I_2$ , as it was difficult to avoid contact with air during the sample dilution procedure and the UV-Vis measurements.

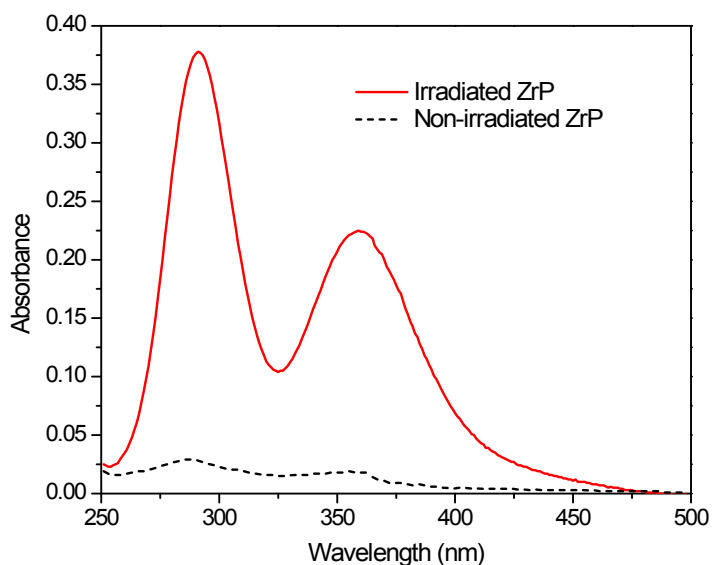


Fig. S2 UV-Vis spectra measuring the amount of  $I_2$  produced by irradiated and non-irradiated ZrP.

When the ZrP platelets (0.03 g/mL) were irradiated with  $^{60}Co$   $\gamma$ -rays in the presence of oxygen, peroxides, X-OOR, and X-OOH, where X stands for the ZrP platelets, and R stands for a short alkyl group from tetrabutylammonium (TBA), were formed on the surface of the ZrP platelets, and also on the TBA chains, which were attracted to the surface of ZrP platelets by the amine groups. The pre-irradiated polymerization was previously used to make composite hydrogels,<sup>3</sup> where the peroxide groups were proven using the iodometry method to be fabricated successfully using organic chemicals with  $^{60}Co$   $\gamma$ -rays under the  $O_2$  ambience.

Poly N-isopropylacrylamide (PNIPAM) was fabricated by initiation of free radicals generated from the hemolysis of peroxide groups on ZrP surface and TBA groups, which attached to the ZrP surface. Each peroxide group was decomposed into two free radicals ( $XO\cdot$

and HO·/RO·) by heating to 50°C under the N<sub>2</sub> atmosphere. The free radicals on the ZrP surface (XO·) would initiate the free radical polymerization of the *N*-isopropylacrylamide monomer to form PNIPAM grafted on the ZrP platelets. Similarly, the peroxide groups on the TBA group will decompose and initiate monomers to form PNIPAM.

Upon completion of the 24-hour reaction, a white viscous suspension product was formed. The product became more transparent and less viscous when it was cooled to room temperature (20°C). The temperature-dependent behaviors indicated the success in the fabrication of PNIPAM polymers, which was further confirmed by the FTIR measurements. The as-prepared ZrP-PNIPAM suspensions were washed twice with deionized water, removing most of the free PNIPAM polymers produced by the small radicals (HO·/RO·) that were not on the ZrP surfaces. After washing, the ZrP-PNIPAM became clearer, and was used as the mother suspension for all further experiments.

FTIR (Fourier transform infrared spectroscopy) was performed using a Bruker Tensor 27 spectrometer in an attenuated total reflection (ATR) mode with a diamond ATR Prism Model Helios. The FTIR spectrum of ZrP and ZrP-PNIPAM platelet suspensions are shown in Fig. S3. We observed the characteristic bands corresponding to the PNIPAM chains: the band for -C=O at 1624 cm<sup>-1</sup> and the band for N-H at 1542 cm<sup>-1</sup>, which did not appear for the ZrP sample, thus proving that the PNIPAM had been successfully grafted onto the ZrP surface using the pre-irradiated polymerization.

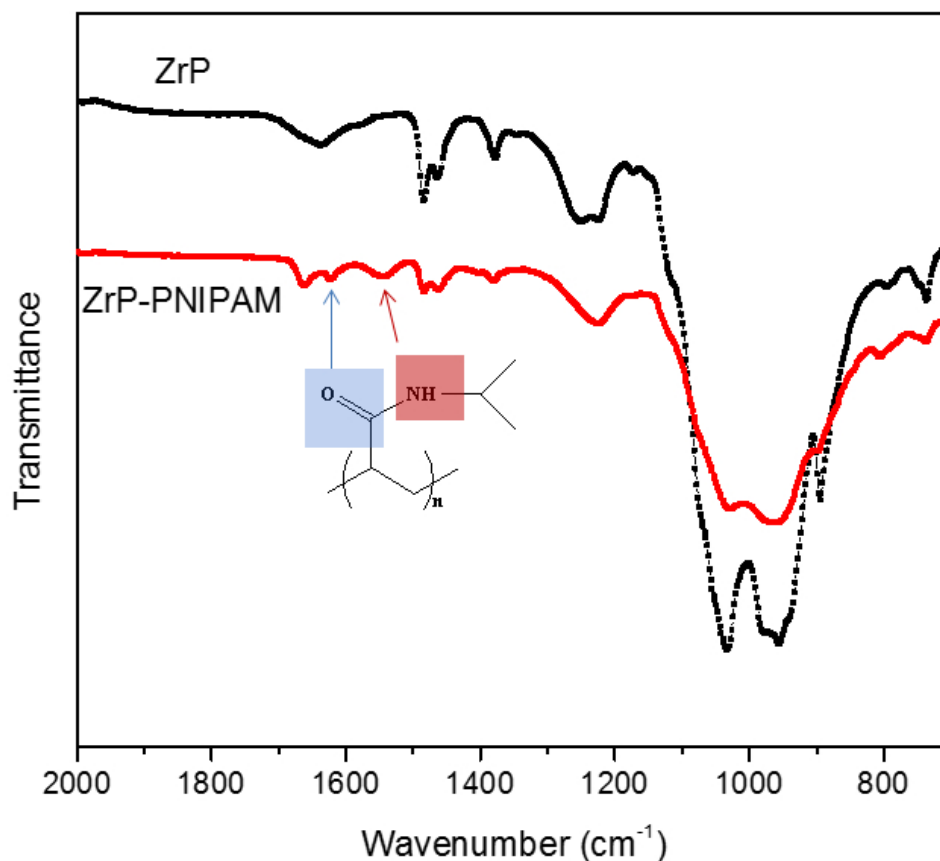


Fig. S3 FTIR spectra of both TBA-exfoliated ZrP and ZrP-PNIPAM.

### 3. Conversion of ZrP-PNIPAM concentration to volume fraction

The volume fraction for the mother suspension was calculated as follows: weighing out a certain volume ( $V_1$ ) of ZrP-PNIPAM suspension ( $m_1$ ) and letting the water evaporate to  $m_2$  at 50°C oven, with the weight difference assumed to be free water in the sample. We found the following: the mass of water  $M$  is equal to  $m_1 - m_2$ , the volume of water  $V_2$  is equal to  $M/\rho$ , where  $\rho$  is the density of water, 1 g/mL. Then we obtained the volume fraction of the ZrP-PNIPAM sample at 50°C as  $\phi$  which is equal to  $(V_1 - V_2)/V_1$ .

The volume fractions at 20°C and 30°C were converted from their volume fraction at 50°C based upon the thickness ratio since the lateral size was fixed. As we know, the thickness of the ZrP-PNIPAM at 20°C and 30°C was 23.4 and 15.9 times more, respectively, than that at 50°C. The volume fraction of platelets was proportional to their thickness; hence, we obtained volume fractions of the samples at 20°C and 30°C by multiplying their volume fractions at 50°C by 23.4 and 15.9, respectively.

The set of samples for liquid crystal phase diagram were diluted from the mother suspension, so their volume fractions were calculated based on the volume fraction of the mother suspension. For example, in a case of the sample with 50% percent dilution (0.5 mL mother suspension addition to 0.5 mL DI water), the volume fraction of this sample is half that of the mother suspension.

### 4. Sedimentation procedure to obtain the equilibrium nematic fraction for the ZrP-PNIPAM samples

The I-N interface can move when isotropic and nematic phases separate due to density difference. The nematic phase can be compressed with time due to gravity. Cross-polarizing photographs were taken for the samples at a periodic sequence after mixing. Fig. S4a presents the photographs for the 0.012 g/mL sample. The nematic fraction for this sample was obtained by normalizing the measured height of the nematic phase to the measured height of the total sample. A plot of the nematic fraction versus time is shown in Fig. S4b. The equilibrium nematic fraction of the sample was obtained by extrapolating back to time zero, as shown in Fig. S4b. The intercept of the fitting line is  $0.932 \pm 0.001$ , so we fixed 0.932 as the equilibrium nematic volume of this sample.

The first three data points Fig. S3b indicates sedimentation of the grains of nematics. The linear part, from 5,000 min to 12,500 min, indicates the compression of the nematics in gravity. The further decrease of the height of the nematics (Fig. S4b) at time beyond 22,500 min is due to the phase transition from the nematics to another phase, which took place at the bottom part of the nematics. This procedure was used for all the samples at 20°C, 30°C and 50°C.

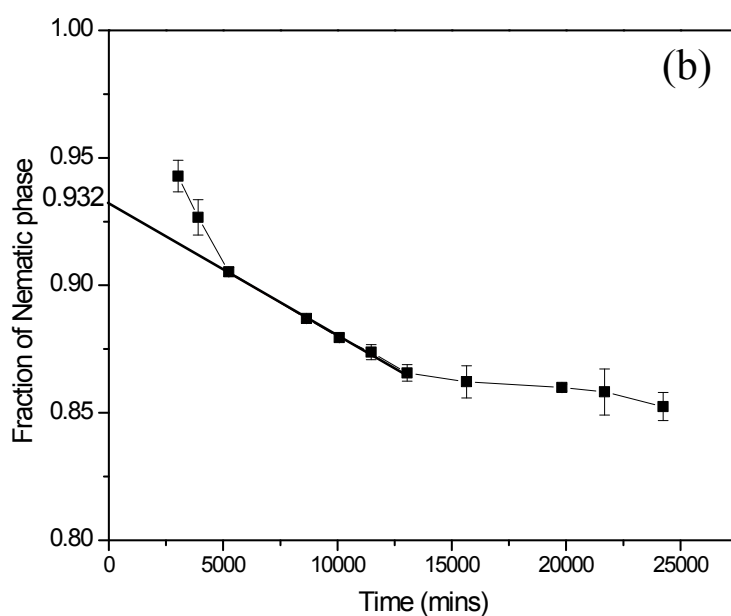
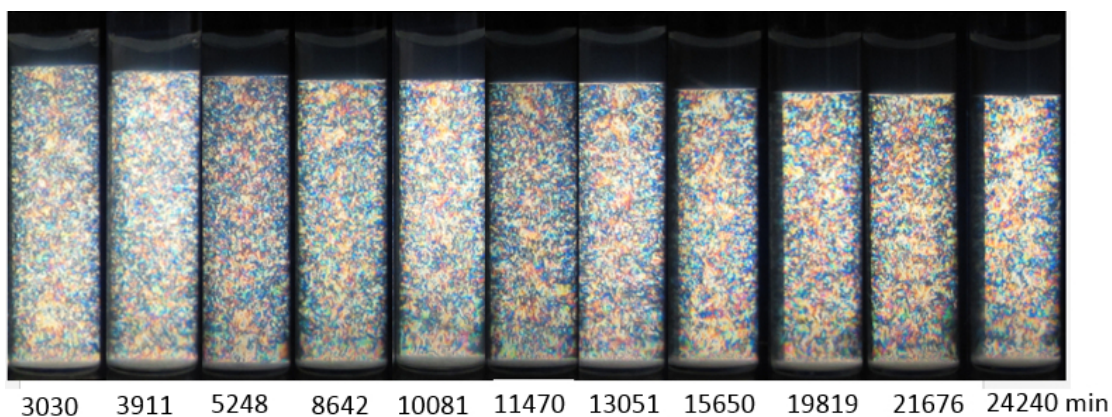


Fig. S4 Determination of the equilibrium nematic fractions of the samples. (a) Cross-polarizing photographs of the 0.012 g/mL sample at 20°C at various times after mixing. (b) The fraction of the nematic phase as a function of time. The solid line indicates the linear extrapolation to time zero after sample mixing.

## 5. Polydispersity effects on ZrP and ZrP-PNIPAM

The size distribution of ZrP monolayers was shown in Fig. S5. By fitting into extreme distribution, we get the polydispersity of the ZrP sample,  $\sigma=24\pm 2\%$ .

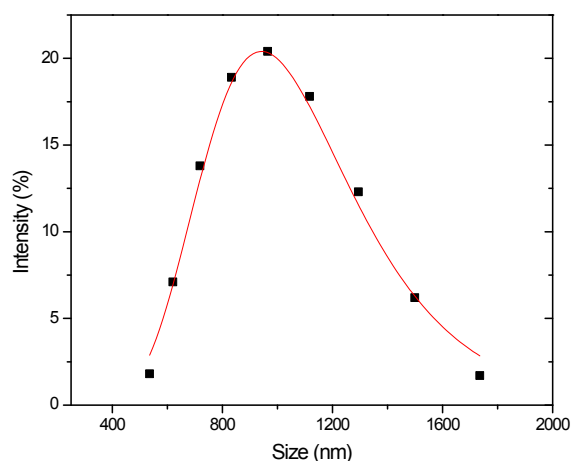


Fig. S5 Size distribution for exfoliated ZrP monolayer as measured by DLS. The lines are fit to the extreme distribution function.

When the temperature increased from 20°C to 50°C, the aspect ratio ( $\xi$ ) of ZrP-PNIPAM platelets decreased from 0.386 to 0.0162, the width of I-N transition became narrower, as shown in points indicated by the star in Fig. S6a, I-N transition width ( $\Delta\phi_{I-N}$ )<sup>4</sup> became smaller. The black and red curves with square symbol in Fig. S5a indicate that the higher the polydispersity, the wider the I-N transition for ZrP. The aspect ratio of ZrP-PNIPAM at 20°C ( $\xi = 0.386$ ) and 30°C ( $\xi = 0.262$ ) were much higher than that of ZrP ( $\xi = 0.01, 0.002$ ), so we were not comparing these two points to ZrP. At 50°C, ZrP-PNIPAM has an aspect ratio of 0.0162, which is closer to that of ZrP at 50°C. We found that for the similar polydispersity,  $\Delta\phi_{I-N}$  of ZrP-PNIPAM was smaller than that of ZrP, as shown by the green star under the black square curve in Fig. S5a. Isotropic volume fraction  $\phi_{I-\xi}$  and nematic volume fraction  $\phi_{N-\xi}$  of ZrP-PNIPAM were also plotted out (Fig. S6b) and compared with ZrP at various polydispersities ( $\sigma$ ) in Fig. S5c. It was obvious that as the aspect ratio became larger and larger, the I-N transition was wider and wider, as shown in Fig. S5b.

Again, as shown in the curves of Fig. S6c, the higher the polydispersity, the wider the I-N transition. The black line in Fig. S5c indicates the  $\phi_{I-\xi}$  of ZrP. The  $\phi_{N-\xi}$  of ZrP is shown as the dashed, dotted and alternating dash-dot lines as the polydispersity increased. The dash-dot line was the furthest one away from the black line, while the dot line was the nearest one, which indicates that the distance between the  $\phi_{I-\xi}$  and  $\phi_{N-\xi}$  lines increased as the polydispersity increased for ZrP. As shown in Fig. S6c,  $\phi_{I-\xi}$  line of ZrP-PNIPAM was paralleled to its  $\phi_{N-\xi}$  line in the log-log plot, which was the same as ZrP did, and the parallelism which was consistent with the  $\phi-\xi$  lines for ZrP.

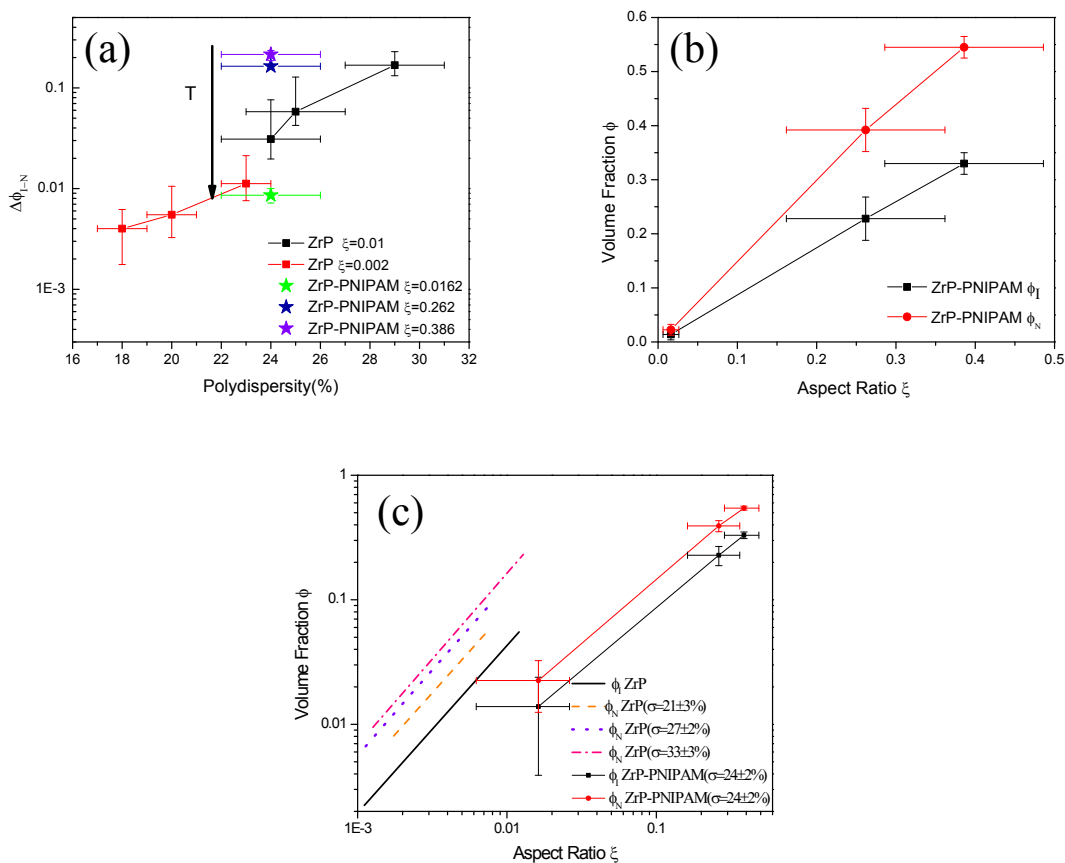


Fig. S6. (a)  $\Delta\phi_{I-N}$ - $\sigma$  of ZrP at different temperatures compared with ZrP samples at two different aspect ratios, 0.01 and 0.002<sup>4</sup>, (b)  $\phi_I$ - $\xi$  and  $\phi_N$ - $\xi$  of ZrP-PNIPAM, (c) log-log plot of  $\phi_I$ - $\xi$  and  $\phi_N$ - $\xi$  for ZrP-PNIPAM, comparing with ZrP with various polydispersities<sup>4</sup>.

## References

- 1 A. F. Mejia, R. Ng, P. Nguyen, M. Shuai, H. Y. Acosta, M. S. Mannan and Z. Cheng, *Soft Matter*, 2013, **9**, 10257-10264.
- 2 Y. Wang and H. L. Wang, *Radiation Physics and Chemistry*, 2009, **78**, 234-237.
- 3 T. Huang, H. Xu, K. Jiao, L. Zhu, H. R. Brown and H. Wang, *Advanced Materials*, 2007, **19**, 1622-1626.
- 4 A. F. Mejia, Y. W. Chang, R. Ng, M. Shuai, M. S. Mannan and Z. D. Cheng, *Phys. Rev. E*, 2012, **85**, 061708.